The Potential Role of Addition Coupled Electron Transfer (ACET) in Single Atom Catalysis: The Hydrogen Transfer from Metalloporphyrin to Imine is an ACET

Yumiao Ma*[a,b] and Aqeel A. Hussein*[c]

a. BSJ Institute, Haidian, Beijing, 100084, People's Republic of China. ymma@bsj-institute.top
b. Hangzhou Yanqu Information Technology Co., Ltd. Xihu District, Hangzhou City, Zhejiang Province, 310003, People's Republic of China
c. Department of Biomedical Science, College of Science, Komar University of Science and Technology, 46001 Sulaymaniyah, Kurdistan Region, Iraq; Email: aqeel.alaa@komar.edu.iq

Abstract: The formal hydrogen transfer from single atom catalyst to unsaturated compounds is of great interest in the catalysis research. With the hydrogen transfer from metalloporphyrin hydride (MPcH, M = Fe, Co) to imines as an example, we have shown that this reaction is an addition coupled electron transfer (ACET) reaction instead of a hydride transfer, by combining density functional theory (DFT), multireference calculations, intrinsic reaction coordinate analysis and substituent effect study. The ACET mechanism is universe in both low-polar solvent (dichloromethane) and high-polar protic solvent (2-propanal). The barrier versus Hammett substituent constant relationship under dichloromethane solvation features a volcano-like shape, in which both electron-withdrawing and electron-donating groups accelerates the reaction. While the structure-reactivity relationship cannot be rationalized by either substituent constant σ_p or the spin delocalization constant σ_{JJ}, it can be successfully explained by a theoretical model of ACET proposed by us for the first time in this work. This work shows that ACET may be ubiquitous in single atom catalyzed addition reactions.

Introduction

Since its first being proposed in 2011,[1] the field of single atom catalysis [2-4] has been keeping growing and has become one of the topics of the highest interest in current chemistry. In a single atom catalyst (SAC), a metal atom is highly dispersed and anchored on a solid surface with generally strong covalent bonding, rendering the chemical environment of the active site well-defined and tunable, which opens a door to a more understandable and controllable catalysis behavior. Single atom catalysts have been applied for the hydrogenation of unsaturated substrates containing C–C, C–N or C–O multiple bonds (Figure 1b-i).[5-11] Due to its high importance, the mechanistic understanding on the key elementary steps in the related reactions is expected to play a key role in understanding the reactivity and rationale design of new catalysts. In most of the single atom catalyzed hydrogenation reaction, a formal hydrogen transfer is proposed to occur from a metal hydride to the unsaturated substrates.[8, 12] In this work, we focus on this step, and found that it belongs to a new type of elementary step, namely the Addition Coupled Electron Transfer (ACET), which was proposed by us in 2021.[13, 14] In an ACET reaction, an addition event into a multiple bond is promoted by a single electron transfer (ET), and these two events are coupled in one single elementary step. The presence of ET plays an essential role in activating the addition reaction, especially for weak nucleophilic reagent or unactivated multiple bonds. The first example of ACET proposed by us was an imaginary nucleophilic addition into a biquinone system (Figure 1a-i), in which the addition into one of the two benzoquinone rings is coupled and accelerated by the intramolecular ET into another benzoquinone ring. Later on, we proposed that a formal Diels-Alder reaction between 1,2-diimine and unactivated alkenes could be significantly promoted in the presence of an oxidant, following the ACET mechanism (Figure 1a-ii). Although these reactions are artificially designed in order to set up the presence of ACET as an elementary step, in this work, however, we are going to show that ACET is not far away from practical chemical reactions. On the contrary, it is hidden among some of the most well-known and practically important

reactions.

In this work, with a metalloporphyrin hydride (MPcH, M = Fe, Co), as a model molecule of the single atom catalyst, we studied the hydrogen transfer into a series of imines, and found that the overall reaction is an ACET rather than a hydride transfer (Figure 1b). These reactions feature a unique volcano-like Hammett relationship, which could not be understood by the previously-known substituent constants. According to our basic understanding on the ACET process, we proposed a theoretical model for the barrier of an ACET reaction, which well rationalized the observed barrier-substituent relationship.

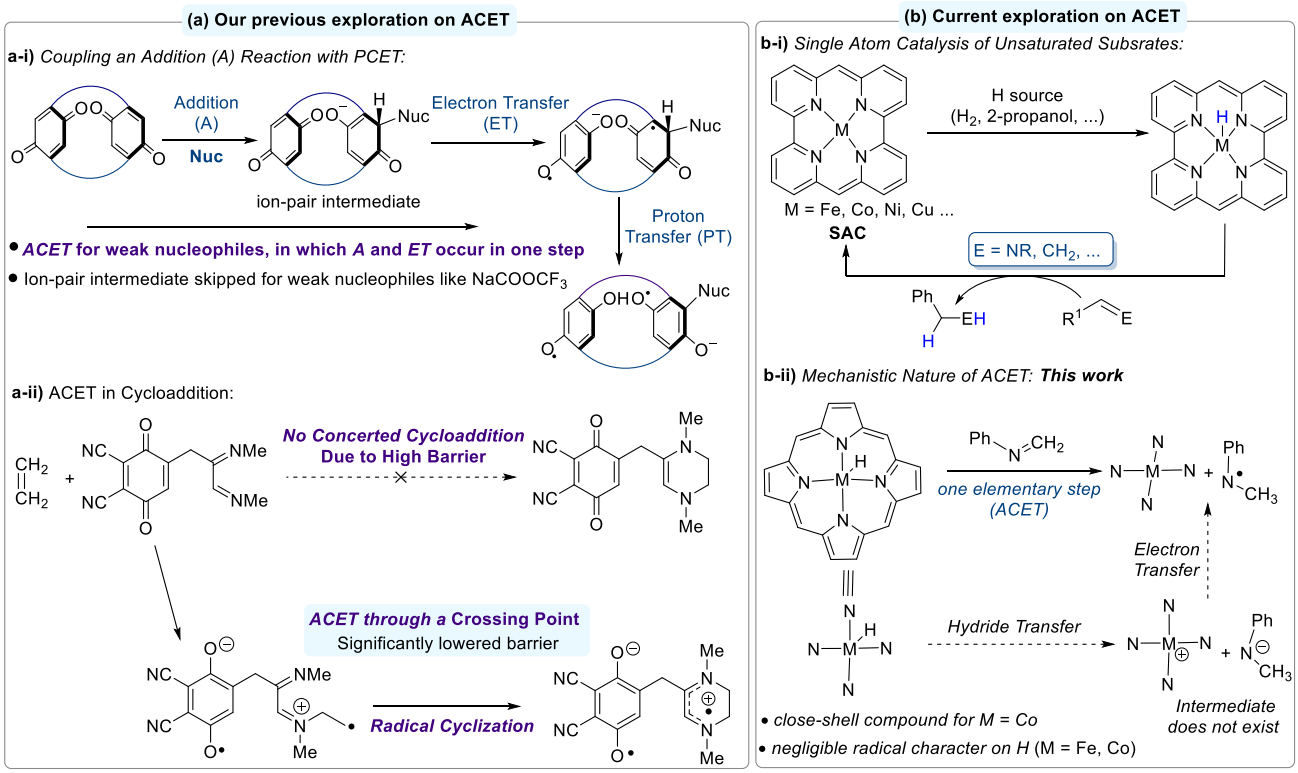

Figure 1. A schematic representation of this work.

Computational Methods

All computations were conducted in Gaussian 16 [15] with the Gaussian 09 default integral grid. The recently designed DFT global hybrid functional MN15 [16] was used for all calculations. Geometry optimization of all structures was performed with the def2-SV(P)[17] basis set, and followed by frequency calculations to obtain Gibbs free energy correction at room temperature. All the intermediates were verified by the absence of negative eigenvalues in the vibrational frequency analysis while all the transition state structures being verified through having a single imaginary frequency. Single point calculations were performed with the def2-TZVP basis set to account better accuracy of the results. The implicit solvation model based on density (SMD) was employed in both the geometry optimization and single point calculation with dichloromethane (DCM) as the solvent medium, if not specially noted.[18] The stability of wavefunction was checked for all the structures involved in this study. The spin density was plotted with the Multiwfn program.[19] The molecular geometry and isosurface were plotted with CYLView[20] and VMD.[21] The multireference calculations within the Complete Active Space SCF (CASSCF) method were performed using the BAGEL program,[22] in combination with the def2-TZVPP basis set.

Results and Discussions

In this work, in order to reveal the reaction mechanism of the hydrogen transfer from transition metal hydrides anchored on a planar square ligand, we focus on two selected metal center, namely Fe and Co. While both are commonly used in single atom catalysis, they represent two different classes of metal complex, with an odd and even number of total electrons, respectively. The cobalt porphyrin hydride (CoPcH) and ferroporphyrin hydride (FePcH) **4** were selected as the model of the single atom catalysts, because they are both derivatives of structurally well-defined molecules (metalloporphyrins), which share similarity with the typical planar-square MN_4 type single atom catalysts. Our simulations were performed at the (SMD/DCM)-MN15/def2-TZVP//(SMD/DCM)-MN15/def2-SV(P) level of theory, whereas in the later section the conclusions will be validated under solvation of 2-propanol as a solvent with much larger dipole.

Reaction Mechanism. According to the DFT results, both CoPcH **1** and FePcH **4** adopt a low-spin ground state. Specifically, **1** exhibits a closed-shell singlet ground state, with no radical character on both Co and H atom (Figure 1a). The CASSCF calculation with a large active space (12 electrons and 12 orbitals) agrees that the ground state is indeed almost closed-shell, as indicated by the high contribution from the electronic configurations in which all the occupied orbitals are doubly occupied (95.6%). The lowest triplet state is quite high in energy, as shown by the triplet energy relative to the ground state is 41.6 and 35.7 kcal/mol at CASSCF and MN15 level, respectively. The Hirshfeld charge [23] at MN15 level shows that the hydrogen atom is slightly negative (-0.026), as compared to the Co atom with atomic charge of +0.111. All of these observations disclose that the ground state of CoPcH **1** is a hydride complex of Co(III) that has no radical character (Figure 1a).

Even though FePcH **4** has an odd number of electrons, it shares quite similar electronic structure with **1**. The unpaired electron at MN15 level is almost concentrated on the Fe atom, as indicated by the low spin population on H (-0.129, versus 1.242 on Fe). In order to further reveal the distribution of radical character on the more reliable CASSCF level, an odd electron density (OED)[24] isosurface was plotted (Figure 2c, d). As the OED is a method to visualize the distribution of radical distribution based on high-quality post-Hartree Fock density matrix, it is clear that the hydrogen atom bears only negligible radical character in both **1** and **4**.

Both the reaction of **1** and **4** occurs through the low-spin state (Figure 2e, f). Naively, one may expect that a closed-shell compound **1** should undergo a nucleophilic addition into an imine substrate, giving an ion-pair intermediate (Figure 1), and the hydride complex **4** with negligible radical character on H should behave similarly. However, the actual results are on the contrary. Despite the closed-shell hydride nature of **1**, the reaction of **1** with imine substrate **2** gives an open-shell singlet product **3** instead of the ion-pair expected for a hydride transfer (Figure 2e). The suspicious closed-shell "ion-pair intermediate" is not a minimum on the PES, and even do not correspond to a stable wavefunction (the closed-shell state is 40.8 kcal/mol above the open-shell singlet state). The reaction proceeds through an open-shell singlet transition state (TS) ^{1}**TS1** with a barrier of 12.5 kcal/mol. The spin density isosurface clearly shows that both ^{1}**TS1** and its product ^{1}**3** are biradical at both the Co atom and the imine fragment (Figure 3a). In **TS1**, the biradical character is relatively small (S**2 = 0.2424), while the S**2 increases dramatically to 1.0458 in ^{1}**3**. The biradical nature of **3** clearly reveals that an electron transfer must occur during the nucleophilic addition of the hydride complex **1** into the imine substrate. The reaction for **4** is quite similar, with a barrier of 12.0 kcal/mol, affording the radical-pair product **5** in which the unpaired electron lies on the Fe and the imine N atom (Figure 3b). As a result, both the "hydride addition" of CoPcH **1** and FePcH **3** is coupled with an ET, from the nitrogen atom into the metal center.

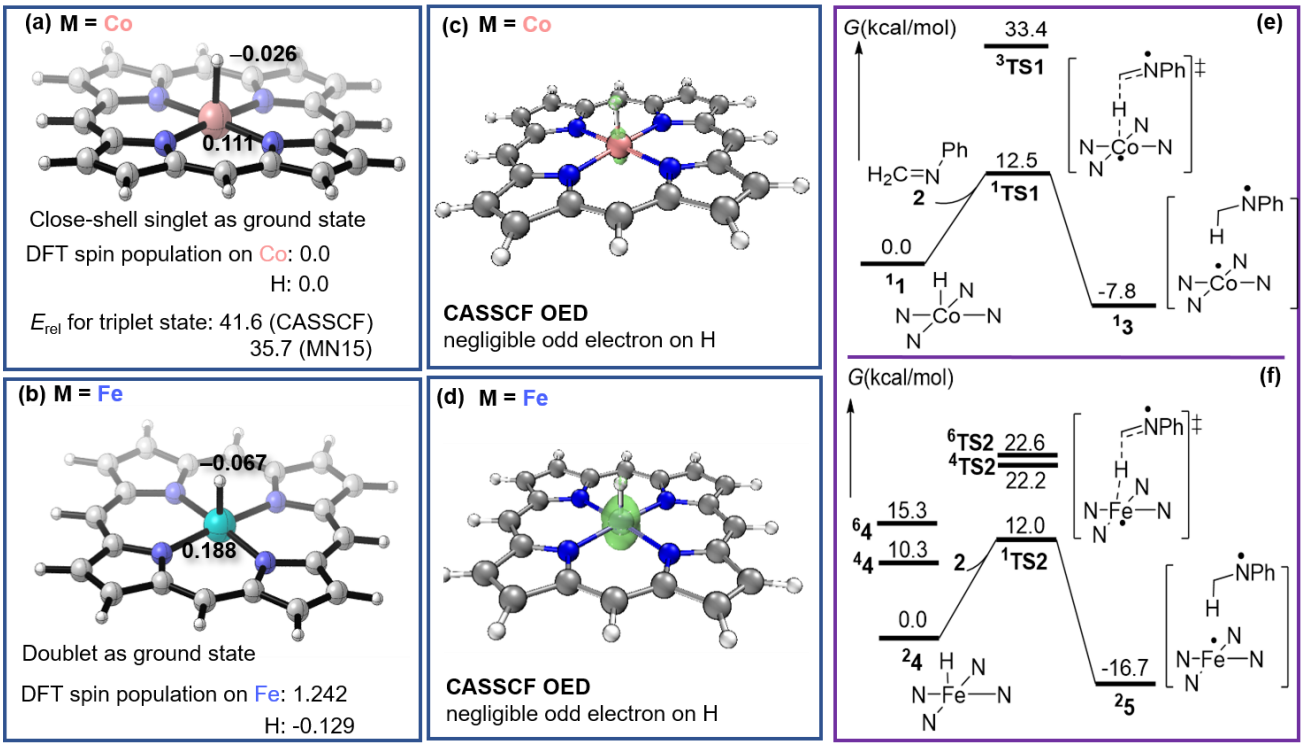

Figure 2. (a, b) The structure of CoPcH ^{1}**1** (a) and FePcH ^{2}**4** (b). The Hirshfeld atomic charges are labelled on the interested atoms. (b). (c, d) The odd electron density (OED) isosurface (isovalue is set to 0.03) at CASSCF(12,12)/def2-TZVPP level for **1** (c) and **4** (d). (e, f) The Gibbs free energy profile for the hydrogen transfer reaction between imine **2** and **1** (e) and **4** (f).

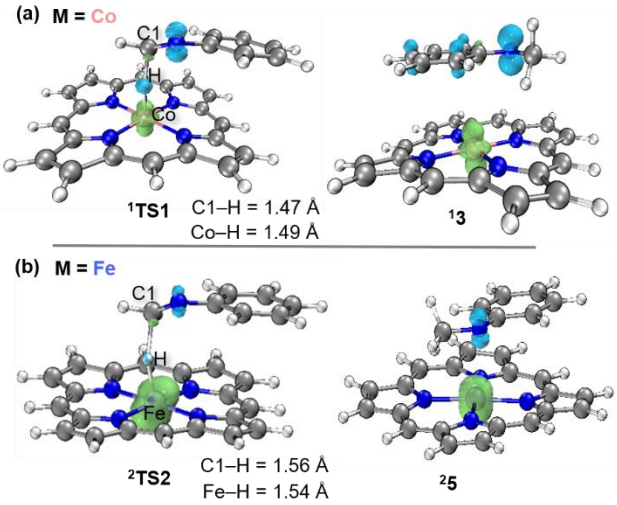

Figure 3. Spin density isosurfaces for selected species along the hydrogen transfer reaction.

In order to gain further insights of the electronic nature of the reaction, an intrinsic reaction coordinate (IRC) calculation was performed, along which the key spin population and atomic charge were recorded and depicted in Figure 4. Interestingly, the energy curve along the IRC exhibits a sharp change near the transition state for both **TS1** (Figure 4a) and **TS2** (Figure 4b), different from a common chemical reaction in which the energy curve becomes flat at the point of TS. Furthermore, the change of spin population on the imine N atom along the IRC pathway also

shows a sharp change from zero to around 0.6~0.7 once the TS is reached. The observations on the spin population curve confirms that an electron transfer (ET) event occurs at exactly the point of **TS1** and **TS2**, and therefore the TS is better considered to be the crossing point between the non-ET and ET potential energy surfaces (PESs).

The addition and ET events can be further identified from the Hirshfeld charge curve (Figure 4e,f), in which the evolution of the atomic charge on the imine nitrogen is depicted. Before **TS1** or **TS2** is reached, a negative charge keeps accumulating on the imine N, and reaches its maximum (~–0.17) at the position of TS. The developing of negative charge is in consistence with a hydride transfer at the stage before the TS is reached. A sharp loss of negative charge occurs, however, at the point of TS, which clearly shows the presence of an instant ET event in which one electron is transferred from the anionic N atom to the metal center. Overall, all the observations above show that the hydrogen transfer from **1** to imine proceeds through an ACET mechanism, in which the hydride addition and a single electron transfer is coupled in one single elementary step.

Effect of Solvation Polarity. Although the above calculations were performed under DCM solvation, a more polar solvent, 2-propanol, which is commonly used in transfer hydrogenation reaction, was also examined (Figure 4g-i). One major concern about ACET is that whether it will be shifted into a traditional hydride transfer when the solvation environment is polar enough or the imine substrate is electronic deficient enough to stabilize the partial negative character on the nitrogen atom produced by hydride addition. Therefore, the 4-nitro substituted imine was selected as the model substrate, in which the strongly electron-withdrawing nitro group is expected to challenge the existence of the ACET mechanism. Furthermore, in addition to the implicit solvation of 2-proponal, an explicit propanol molecule was considered by forming a hydrogen bonding with the imine nitrogen. The corresponding transition state, namely **TS1**(4-NO_2, 2-propanol), was optimized under (SMD/2-propanol)-MN15/def2-SV(P) level, and the IRC was studied as above. In the transition state (Figure 4g), the 2-propanol molecule forms a hydrogen bonding with imine of 1.87 Å, and no proton transfer was observed along the IRC. The energy curve and the spin population curve are quite similar to the DCM case (Figure 4a-f), featuring a sharp change in the energy, a sudden increase in the spin population on the imine N atom, and a clear turning point of atomic charge on N atom at the TS. All these features clearly show that the ACET mechanism is remained even under a polar protic solvent.

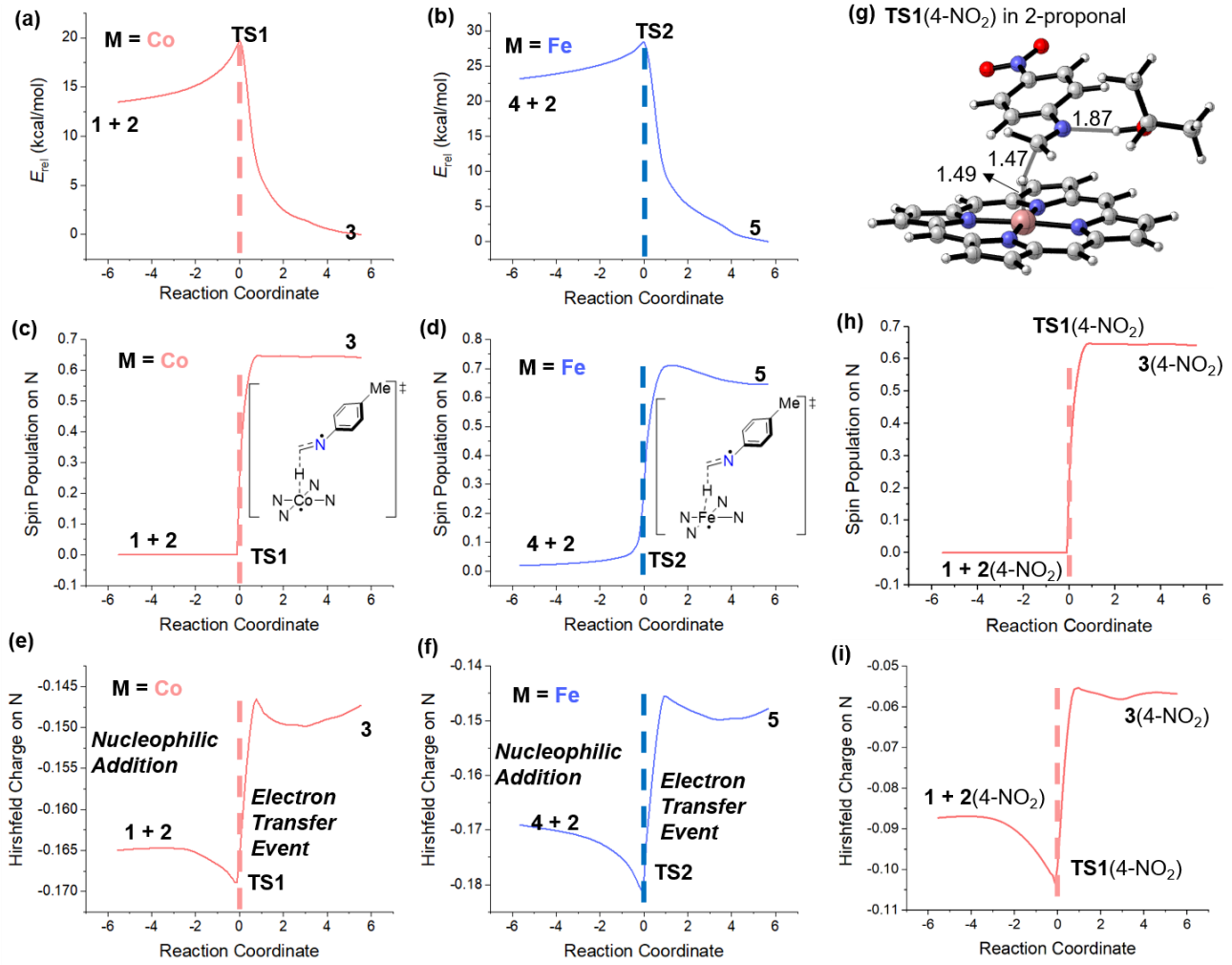

Figure 4. The evolution of (a, b) energy, (c, d) spin population on the imine nitrogen atom, and (e, f) Hirshfeld charge on the imine nitrogen atom along the IRC from **TS1** and **TS2**. (g) The geometry of **TS1**(4-NO_2, 2-propanol), where distances are shown in Å. The evolution of the spin population on the imine N atom along the IRC from **TS1**(4-NO_2, 2-propanol).

Effect of substituents on ACET. After the establishment of the ACET mechanism, we were next interested in the substituent effect on the barrier (Figure 5). For a traditional hydride transfer, it is expected that an electron-withdrawing group (EWG) on the imine substrate promotes the reaction due to the stabilization effect toward the negative charge developed on the imine nitrogen atom. As for the ACET reaction, its Hammett relationship is yet unknown. By studying various 4-substituted imines **2** of both EWG and electron-donating group (EDG), a Hammett relationship was obtained (Figure 5b). All the substrates were determined to react through the ACET mechanism, even for **2**(4-NO_2), in which the strong EWG was expected to stabilize the negative charge generated in the hydride transfer phase. Interestingly, both EWGs and EDRs are shown to decrease the barrier, while a maximum barrier appears when R = Me, resulting in a unique volcano-type relationship between Hammett constant (σ_p) and the barrier (Figure 5b). Obviously, this Hammett relationship is different from a simple polar addition reaction.

Although the radical delocalization constant (σ_{JJ}) [25] is known to have been successfully used to explain the Hammett relationship in some of the radical addition reactions, no satisfactory linear relationship was achieved by a multi-variant regression procedure combining σ_{JJ} and the Hammett constant (σ_p) [26] (Figure 5c). The failure of traditional Hammett regression to rationalize the barrier-substituent relationship further indicate that the reaction has a different

nature from the known polar or radical addition, validating our conclusion that the reaction belongs to a new type of elementary step named ACET. According to these observations, the ACET reaction might does not follow a simple linear free energy relationship. As a result, in the next section, we turned our attention to put forward a theoretical model using two imaginary diabatic PESs in order to give a satisfactory quantitative description of the barriers of ACET reactions.

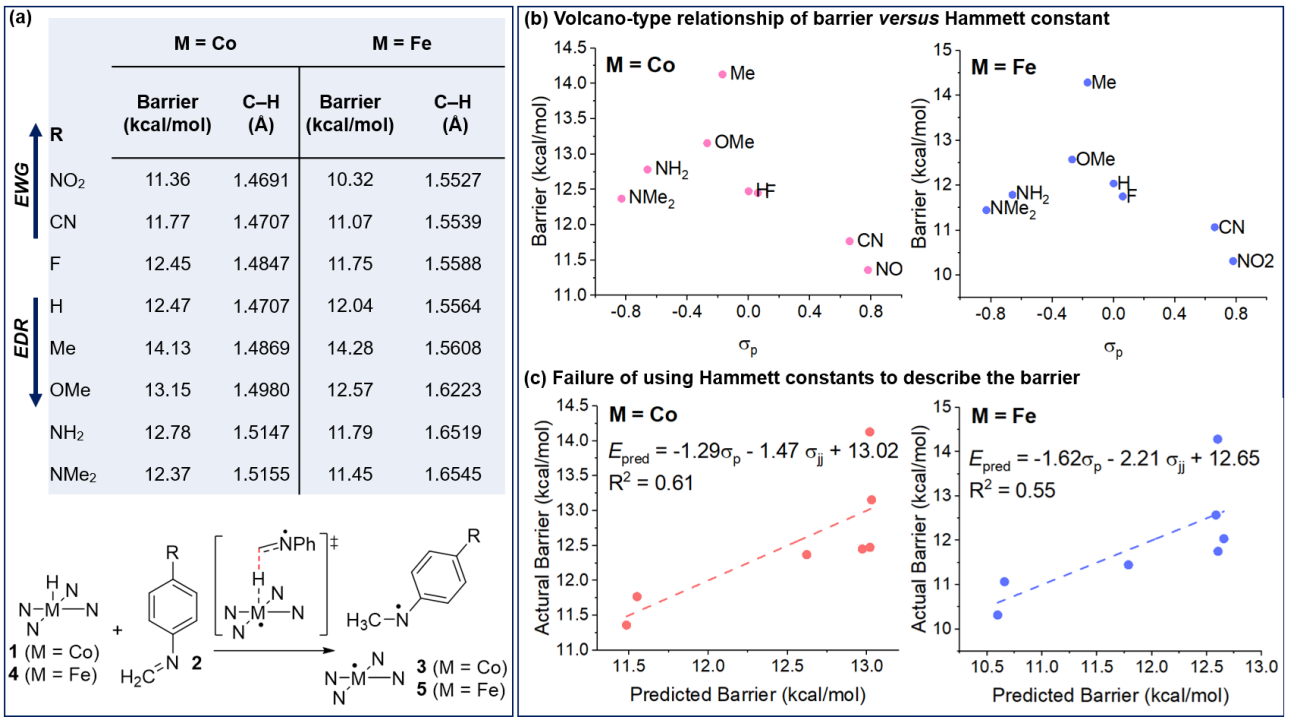

Figure 5. (a) The calculated barrier and C–H bond length in **TS1** or **TS2** for substituted imines (**2**). (b) The barrier versus *para*-Hammett constant σ_p plot. (c) The actual barrier versus the barrier predicted by a multi-variant regression using substituent constant σ_p and σ_{JJ} plot.

The ACET Theoretical Model. To explain the irregular Hammett relationship shown in Figure 5, a theoretical model considering the crossing of two diabatic PESs is proposed. This model is similar to the known theoretical model of proton-coupled electron transfer, but much more simplified, considering only the four critical points of the reaction.[27] The two PESs, namely PES1 and PES2, correspond to the PES for the reaction between metalloporphyrin **MPcH** and imine **2** without and with ET, respectively (Figure 6a). The reaction coordinate is defined by the extent of hydrogen transfer: the hydrogen atom lies on the metal center when the reaction coordinate (x) is zero, and is completely transferred when the reaction coordinate x reaches 1. The real product **3** (when M = Co) or **5** (when M = Fe) is the radical pair consisted of two fragments, noted as **6** and **7**. PES1 is the diabatic PES for a pure hydride transfer, starting from its minimum (**MPcH** + **2**) at the point $x = 0$, and connects an imaginary ion-pair state consisted of the anionic $\mathbf{7}^-$ and the metallic cation $\mathbf{6}^+$ when $x = 1$. On the other hand, the PES2 deals with an imaginary state after the ET from the metal center to the imine substrate. While the radical pair formed by **6** and **7** lies on the minimum of PES2 when $x = 1$, the $x = 0$ point corresponds to the imaginary state $\mathbf{MPcH}^-$ + $\mathbf{2}^+$. In our ACET theoretical model, the real reaction occurs through the adiabatic PES (labelled in bold in Figure 5a) formed by the crossing between PES1 and PES2, and therefore the position and energetics of the TS can be evaluated by solving the crossing point between the two imaginary PESs.

In this scheme, in order to understand the PES crossing behavior to a basic extent, we only need to know the energies

of four points (the point x = 0 and x = 1 on PES1 and PES2, respectively). The starting compound (x = 0), namely **MPcH** + **2**, is the minimum of PES1, which is defined to be the origin point (G_{rel} = 0) in our scheme. The relative energy of the x = 0 point on PES2 can be roughly approximated to be the sum of the vertical electron affinity (EA) of **MPcH** and the vertical ionization potential (IP) of **2**. As for the reaction product on PES2 (reaction coordinate = 1), its relative energy is the overall Gibbs free energy change of the reaction, noted as $\triangle G$, and the energy of the corresponding point on PES1 can be evaluated to be $\triangle G$ + IP(**6**) + EA(**7**), in which **4** and **5** is the product Co(II) porphyrin and the N-radical, respectively, as shown in Figure 5a. Then, the PES1 and PES2 can be approximated to be the quadratic curve through the key species (for convenience, straight lines were used instead in qualitative scheme in Figure 5), and **TS1** is the crossing point between the two PESs.

Qualitatively, we can consider the influence of substitutes as the follows. First of all, we take the non-substituted case as the reference (Figure 5a, center). For any substituent group, EA(**MPcH**) and IP(**6**) are constant. If we take $E1$ = EA(**MPcH**) + IP(**2**), and $E2$ = EA(**7**) + IP(**6**), we will easily know that an EWG will increase $E1$ and decrease $E2$, shifting PES1 flatter and PES2 more precipitous (Figure 6a, right), resulting in a later **TS1** and lower barrier. On the contrary, an EDR raises $E2$ and decreases $E1$, affording an earlier **TS1** and, again, a lower barrier. In this framework, both EWGs and EDRs promote the ACET reaction, in consistence with the observed volcano-type barrier- substituent constant relationship. Furthermore, the prediction on the shifting of the **TS1** position is also validated by the C–H bond length (Figure 5a). The EDR substituted **2** exhibits a significantly longer C–H bond length in both **TS1** and **TS2** (for example, the C–H bond length in **TS1**(p-NMe_2) is 1.5155 Å, as compared to 1.4707 Å for **TS1**(p-H)), indicating an earlier TS, whereas the opposite situation is observed for EWGs.

After the success in qualitatively understanding the substituent effect on the ACET reaction, we next turn to compare the quantitative behavior of our model. The following calculating procedure is used to predict the barrier of an ACET:

1. Optimize the geometry of **MPcH**, **2**, **6**, **7** to derive their vertical EAs and IPs. Calculate $E1$ and $E2$ according to these results. Calculate and the reaction thermodynamics $\triangle G$ for a given substrate **2**.
2. Do a quadratic fitting towards PES1 and PES2, in which x is the reaction coordinate:
   $G1 = (\Delta G + E2)x^2$ ……. (1)
   $G2 = (-\Delta G + E1)(x-1)^2 + \Delta G$ …….(2)
3. Calculate the reaction coordinate x and free energy G of the crossing point by solving $G1 = G2$.

Following the above procedure, the predicted barriers were calculated for all the substituted **2** studied (Figure 6c). Surprisingly, although our theoretical model seems rough and simple, a much better linear relationship between the barriers evaluated by this model and the actual DFT-derived barrier is gained. Although the barrier is systematically underestimated by ~3 kcal/mol, which is quite understandable considering the high simplicity of this model, the R^2 for the reaction of **1** and **4** is determined to be 0.83 and 0.70, respectively, significantly higher than that obtained by multivariant Hammett regression (0.61 and 0.55, Figure 5c). The good linear relationship clearly reveals the success of our model among the examples studied herein. More importantly, as our model is completely derived from our basic physical understanding on ACET, and involves no parameter fitting, its success further supports the ACET nature of these reactions. Overall, according to the theoretical model above, not only can we successfully explain the observed substituent relationship for an ACET reaction, but also are we able to obtain a good qualitative agreement with the DFT-calculated barrier through this simple theoretical model.

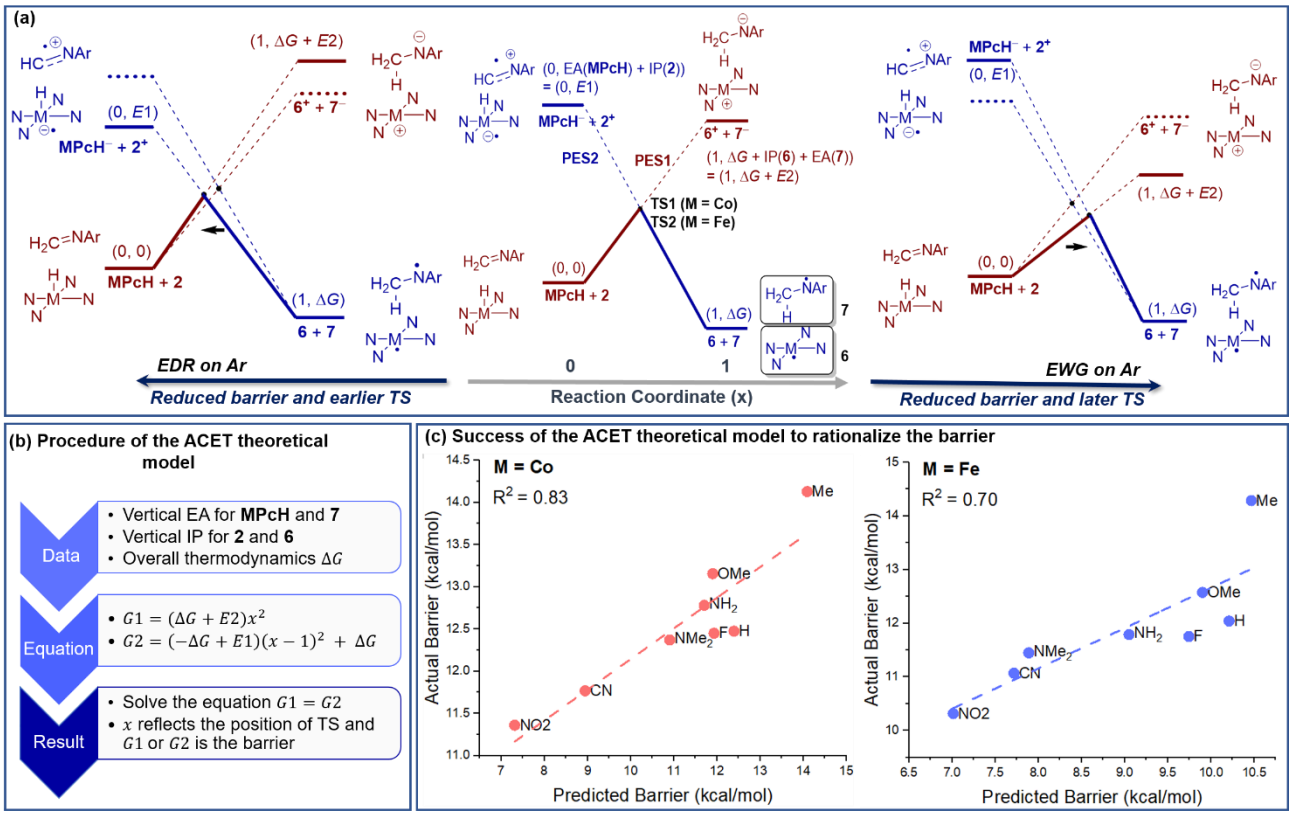

Figure 6. Our theoretical model for ACET reaction (a), the schematic procedure for calculating ACET barrier according to this model (b), and the predicted versus DFT-calculated barrier plot (c).

Conclusion

In this work, taking the hydrogen transfer from two typical metalloporphyrin hydride, namely CoPcH **1** and FePcH **4** to imines as the model reaction, we have shown that this reaction occurs through an ACET mechanism. Electronic structure analysis by combining DFT and CASSCF shows that both **1** and **4** exhibit negligible radical character on the hydrogen atom and, more importantly, **1** is even a closed-shell complex. Although they are best considered to be hydride complexes, the hydrogen transfer reactions from both **1** and **4** to imines give a radical pair product **3** (for CoPcH **1**) or **5** (for FePcH **4**) in one elementary step, significantly different from the hydride transfer product expected based on the hydride nature. The IRC shows clearly that the reaction coordinate is divided into two phases at exactly the point of the TS: within the pre-TS region, the reaction can be considered to be a nucleophilic hydride addition, resulting in developing negative charge on the imine nitrogen atom. Once the TS is reached, a sudden change in both the atomic charge and spin population occurs, leading to a N-radical, which is in consistent with an instant ET event. The nucleophilic addition and ET event are coupled in one elementary step, leading us to conclude that the overall reaction follows an ACET mechanism.

In addition to the mechanistic analysis, we further investigated the substituent effect on the ACET reaction. The reaction exhibits a unique volcano-type Hammett relationship, which cannot be rationalized by linear regression using substituent constants. Instead, we proposed a theoretical model to evaluate the ACET barrier, and successfully rationalized the observed Hammett behavior. This theoretical model makes use of a quadratic modelling of two crossing diabatic PESs, giving a description of the position of TS and its energetics from the IPs and EAs of relevant species. Based on this quite simple but effective model, we are able to understand the substituent effect on the ACET barrier and TS position both qualitatively and quantitively. Specially, the ACET barriers predicted by this model

shows significantly improved linear relationship as compared to the traditional Hammett regression.

The metalloporphyrin system studied here is closely connected to single atom catalysis, because it features a rigid, planar-squared metal center which is shared by most single atom catalysts. We suggest that ACET might be ubiquitous in the group transfer reaction involved by single atom catalysts, as a new type of elementary step which has not been separately studied before.

Acknowledgement

Both authors thank Hangzhou Yanqu Information Technology Co., Ltd for purchasing the license for Gaussian.

References:

1. Qiao, B.; Wang, A.; Yang, X.; Allard, L. F.; Jiang, Z.; Cui, Y.; Liu, J.; Li, J.; Zhang, T., Single-atom catalysis of CO oxidation using Pt 1/FeO x. *Nature chemistry* **2011,** *3* (8), 634-641.

2. Chen, F.; Jiang, X.; Zhang, L.; Lang, R.; Qiao, B., Single-atom catalysis: Bridging the homo- and heterogeneous catalysis. *Chinese Journal of Catalysis* **2018,** *39* (5), 893-898.

3. Wang, A.; Li, J.; Zhang, T., Heterogeneous single-atom catalysis. *Nature Reviews Chemistry* **2018,** *2* (6), 65-81.

4. Yang, X.-F.; Wang, A.; Qiao, B.; Li, J.; Liu, J.; Zhang, T., Single-atom catalysts: a new frontier in heterogeneous catalysis. *Accounts of chemical research* **2013,** *46* (8), 1740-1748.

5. He, X.; He, Q.; Deng, Y.; Peng, M.; Chen, H.; Zhang, Y.; Yao, S.; Zhang, M.; Xiao, D.; Ma, D., A versatile route to fabricate single atom catalysts with high chemoselectivity and regioselectivity in hydrogenation. *Nature communications* **2019,** *10* (1), 1-9.

6. Tian, S.; Hu, M.; Xu, Q.; Gong, W.; Chen, W.; Yang, J.; Zhu, Y.; Chen, C.; He, J.; Liu, Q., Single-atom Fe with Fe1N3 structure showing superior performances for both hydrogenation and transfer hydrogenation of nitrobenzene. *Science China Materials* **2021,** *64* (3), 642-650.

7. Wang, H.; Luo, Q.; Liu, W.; Lin, Y.; Guan, Q.; Zheng, X.; Pan, H.; Zhu, J.; Sun, Z.; Wei, S., Quasi Pd1Ni single-atom surface alloy catalyst enables hydrogenation of nitriles to secondary amines. *Nature communications* **2019,** *10* (1), 1-9.

8. Zhang, J.; Zheng, C.; Zhang, M.; Qiu, Y.; Xu, Q.; Cheong, W.-C.; Chen, W.; Zheng, L.; Gu, L.; Hu, Z., Controlling N-doping type in carbon to boost single-atom site Cu catalyzed transfer hydrogenation of quinoline. *Nano Research* **2020,** *13* (11), 3082-3087.

9. Zhang, Z.; Zhu, Y.; Asakura, H.; Zhang, B.; Zhang, J.; Zhou, M.; Han, Y.; Tanaka, T.; Wang, A.; Zhang, T., Thermally stable single atom Pt/m-Al2O3 for selective hydrogenation and CO oxidation. *Nature communications* **2017,** *8* (1), 1-10.

10. Zhou, P.; Zhang, Z.; Jiang, L.; Yu, C.; Lv, K.; Sun, J.; Wang, S., A versatile cobalt catalyst for the reductive amination of carbonyl compounds with nitro compounds by transfer hydrogenation. *Applied Catalysis B: Environmental* **2017,** *210*, 522-532.

11. Song, J., Co single-atom catalysts enable efficient reductive amination of biomass-derived levulinic acid. *Chem Catalysis* **2022,** *2* (1), 16-18.

12. Wang, H.; Zhang, W.; Liu, Y.; Pu, M.; Lei, M., First-Principles Study on the Mechanism of Nitrobenzene Reduction to Aniline Catalyzed by a N-Doped Carbon-Supported Cobalt Single-Atom Catalyst. *The Journal of Physical Chemistry C* **2021,** *125* (35), 19171-19182.

13. Ma, Y., Addition Coupled Electron Transfer (ACET) and Addition Coupled Electron Coupled Proton Transfer

(ACPCET). *ChemRxiv* **2021**.
14. Ma, Y., Addition Coupled Electron Transfer (ACET) and Addition Coupled Electron Coupled Proton Transfer (ACPCET). **2021**.
15. Frisch, M. J.; Trucks, G. W.; Schlegel, H. B.; Scuseria, G. E.; Robb, M. A.; Cheeseman, J. R.; Scalmani, G.; Barone, V.; Petersson, G. A.; Nakatsuji, H.; Li, X.; Caricato, M.; Marenich, A. V.; Bloino, J.; Janesko, B. G.; Gomperts, R.; Mennucci, B.; Hratchian, H. P.; Ortiz, J. V.; Izmaylov, A. F.; Sonnenberg, J. L.; Williams; Ding, F.; Lipparini, F.; Egidi, F.; Goings, J.; Peng, B.; Petrone, A.; Henderson, T.; Ranasinghe, D.; Zakrzewski, V. G.; Gao, J.; Rega, N.; Zheng, G.; Liang, W.; Hada, M.; Ehara, M.; Toyota, K.; Fukuda, R.; Hasegawa, J.; Ishida, M.; Nakajima, T.; Honda, Y.; Kitao, O.; Nakai, H.; Vreven, T.; Throssell, K.; Montgomery Jr., J. A.; Peralta, J. E.; Ogliaro, F.; Bearpark, M. J.; Heyd, J. J.; Brothers, E. N.; Kudin, K. N.; Staroverov, V. N.; Keith, T. A.; Kobayashi, R.; Normand, J.; Raghavachari, K.; Rendell, A. P.; Burant, J. C.; Iyengar, S. S.; Tomasi, J.; Cossi, M.; Millam, J. M.; Klene, M.; Adamo, C.; Cammi, R.; Ochterski, J. W.; Martin, R. L.; Morokuma, K.; Farkas, O.; Foresman, J. B.; Fox, D. J. *Gaussian 16 Rev. C.01*, Wallingford, CT, 2016.
16. Yu, H. S.; He, X.; Li, S. L.; Truhlar, D. G., MN15: A Kohn–Sham global-hybrid exchange–correlation density functional with broad accuracy for multi-reference and single-reference systems and noncovalent interactions. *Chemical Science* **2016,** *7* (8), 5032-5051.
17. Weigend, F.; Ahlrichs, R., Balanced basis sets of split valence, triple zeta valence and quadruple zeta valence quality for H to Rn: Design and assessment of accuracy. *Physical Chemistry Chemical Physics* **2005,** *7* (18), 3297-3305.
18. Marenich, A. V.; Cramer, C. J.; Truhlar, D. G., Universal solvation model based on solute electron density and on a continuum model of the solvent defined by the bulk dielectric constant and atomic surface tensions. *The Journal of Physical Chemistry B* **2009,** *113* (18), 6378-6396.
19. Lu, T.; Chen, F., Multiwfn: a multifunctional wavefunction analyzer. *Journal of computational chemistry* **2012,** *33* (5), 580-592.
20. Legault, C., CYLview, 1.0 b. *Université de Sherbrooke* **2009,** *436*, 437.
21. Humphrey, W.; Dalke, A.; Schulten, K., VMD: visual molecular dynamics. *Journal of molecular graphics* **1996,** *14* (1), 33-38.
22. Shiozaki, T., BAGEL: Brilliantly Advanced General Electronic-structure Library. *WIREs Computational Molecular Science* **2018,** *8* (1), e1331.
23. Hirshfeld, F. L., Bonded-atom fragments for describing molecular charge densities. *Theoretica chimica acta* **1977,** *44* (2), 129-138.
24. Nakano, M.; Fukui, H.; Minami, T.; Yoneda, K.; Shigeta, Y.; Kishi, R.; Champagne, B.; Botek, E.; Kubo, T.; Ohta, K.; Kamada, K., (Hyper)polarizability density analysis for open-shell molecular systems based on natural orbitals and occupation numbers. *Theor. Chem. Acc.* **2011,** *130* (4), 711-724.
25. Jiang, X.-K., Establishment and Successful Application of the σJJ• Scale of Spin-Delocalization Substituent Constants. *Accounts of chemical research* **1997,** *30* (7), 283-289.
26. Hansch, C.; Leo, A.; Taft, R., A survey of Hammett substituent constants and resonance and field parameters. *Chemical reviews* **1991,** *91* (2), 165-195.
27. Hammes-Schiffer, S., Theoretical Perspectives on Proton-Coupled Electron Transfer Reactions. *Acc. Chem. Res.* **2001,** *34* (4), 273-281.